Magneto-mechanical behavior of elastomeric carbonyl iron particles composite foams produced by foam injection molding

Valentina Volpe[1], Marco D'Auria[2,3], Luigi Sorrentino[2], Daniele Davino[2,3], Roberto Pantani[1*]

[1]*Department of Industrial Engineering. University of Salerno*

Via Giovanni Paolo II, 132, 84084 Fisciano (SA), ITALY

[2]*Institute of Polymers, Composites and Biomaterials (IPCB - CNR) Piazzale E. Fermi 1, 80055 Portici (Na), Italy*

[3]*Department of Engineering. University of Sannio,*

Piazza Roma, 82100 Benevento, Italy.

[*]*Corresponding author: rpantani@unisa.it*

List of highlights

- Foams made of thermoplastic elastomers reinforced with carbonyl iron particles were produced by foam injection molding.
- Carbonyl iron micro-particles allowed a remarkable improvement of the cellular morphology by strongly increasing the number of nucleated cells without increasing the final density.
- Carbonyl iron micro-particles imparted sensitivity to external magnetic field, making the lightweight composite material "smart".

Keywords: soft magnetic composite; magnetoactive elastomer; magnetoelastic foams; injection molding, thermoplastic elastomer

Abstract. Foamed composite materials based on two thermoplastic elastomers reinforced with carbonyl iron particles (CIP) at 2 % by volume were prepared by using foam injection molding. Nitrogen was used as physical blowing agent. Specimens were characterized by density measurements and morphological analysis. Foams based on neat polymers showed a well-developed cellular morphology only far from the injection point. On the contrary, composite foams showed a considerably increased homogeneity of the cellular structure morphology, with small cells found since the injection point. The magneto-elastic characterization of samples showed that reinforced samples (both unfoamed and foamed) showed a magneto-elastic behavior under a simultaneous application of a pre-strain and a magnetic field: the magnetic field induced response exhibited a butterfly shaped trend, typical of magnetostrictive materials.

Keywords. Tailor-made polymers, foam injection molding, magneto-sensitive elastomers

1. INTRODUCTION

Low density magnetic materials are very promising since they satisfy the need for lightweight smart materials with properties tunable by means of external stimuli. In the scientific literature several magnetorheological (MR) composites based on polymers and aligned magnetic particles (MP) are proposed, but their high density implies the need for very high (1 Tesla) magnetic fields (MF) to optimally distribute the particles, thus reducing their potential application fields. Magnetosensitive foams were prepared by Sorrentino et al. in 2008 by

using a thermosetting polymer (polyurethane) and iron particles [1]. Differently from thermosetting polymers, thermoplastics elastomers (TPE) present several advantages in terms of reduced environmental impact, wastes, absence of volatile organic monomers or by-products, and have the potential for much higher productivity and higher performance/cost ratio. TPE reinforced with CIP had shown promising magnetic and magneto-elastic properties [2, 3].

Foam injection molding is one of the most suitable approaches to produce foams. They are characterized by a sandwich like structure (solid external skins surrounding an inner foam core). A chemical or physical blowing agent is dispersed into the cylinder of the injection molding machine during the supplying phase and after a proper cycle time the compound is injected in the mold cavity where it expands due to the decreasing in pressure after the inlet [4]. The resulting structural foam is characterized by a controlled porosity and a reduction in density typically ranging from 20 to 30 % with respect to the corresponding unfoamed part [5]. Furthermore, higher specific mechanical properties, improved dimensional stability and higher product quality can be obtained [6].

A fundamental aspect of the foam injection molding process is the control of the foam morphology. The promotion of a homogeneous bubble nucleation is typically attained by means of nucleating agents, which promote the formation of bubbles on the nucleating agent surface thus inducing a fine cell size distribution. Several authors studied the effects of the microparticles addition on the mechanical properties and on the cell morphology of foamed parts. In fact, it was demonstrated that the addition of small amounts of reinforcing particles to the polymer enhances mechanical properties, such as Young's modulus and tensile strength, with respect to neat polymers [7, 8].

Thermoplastic elastomers (TPE) are a very promising class of soft polymers. They are characterized by the presence of two phases, a flexible one, providing a rubber-like response

in the solid state, and a rigid one, with a high glass transition temperature or a semicrystalline structure [9].

The presence of suitable particles in the polymeric matrix can impart sensitivity to external stimuli, such as in the case of magneto-rheological (MR) materials. MR materials contain micron-sized ferrous particles dispersed in a (fluid or solid) medium. The application of a magnetic field (MF) allows to change their viscoelastic properties in a continuous, fast and reversible way. Differently from MR fluids, MR solids (like gels, elastomers, and foams) can be easily shaped and their shape is retained after the shaping process [10]. Furthermore, the positioning of particles in magneto-sensitive (MS) solids is fixed during the molding process and thus they cannot freely move within the polymer. The resulting spatial distribution of particles can be either isotropic or anisotropic, depending on whether the particles are aligned by an external MF applied during the consolidation of the polymer or not. MS materials produced by simply dispersing the particles show an isotropic distribution of particles. The magneto-sensitive effect is related to the shape or elastic response variation of such materials under the application of an external MF. The magneto-sensitive effect can be positive (elongation or stiffening) or negative (contraction or softening) in respect to the direction of the applied MF [11]. According to a microscopic approach, magnetic particles are considered separated from each other by a non-magnetic matrix. Dipole-dipole interactions between non-contacting magnetic particles induce the attraction and repulsion of the particles according to their mutual positioning in the polymeric matrix. Since the dependence of the dipole-dipole interaction is strongly dependent on the mutual position of magnetic particles, their spatial distribution can significantly affect the type of magneto-sensitive effect, as shown in simulating and in experimental works [12, 13]. For example, MS materials with isotropic spatial distribution of particles show a contraction-like behaviour along the MF direction,

while MS materials with a distribution of aligned particles show an uniaxial elongation-like or strengthening effect [14, 15].

In this work, a preliminary study on foams, reinforced with CIP and produced by foam injection molding technology, have been investigated. The role of microparticles to improve the cellular morphology in injection molded foams has already been exploited in literature, but CIP micro-particles have been used for simultaneously increase the cellular morphology and, for the first time, to make injection molded foams sensitive to an external stimulus, namely the magnetic field in this case. The effect of iron micro-particles have been investigated in regard to the foam morphology and the mechanical behavior of molded samples under the application of a magnetic field. [16].

2. EXPERIMENTAL SECTION

2.1 Materials, geometry and conditions

Two different thermoplastic elastomers were used in this work: a polyolefin elastomer, ENGAGE 8445 (referred to as ENGAGE in the following) supplied by DuPont Dow Elastomers (Midland, Michigan, USA) and an ethylene vinyl acetate copolymer (referred to as EVA in the following) grade 1040VN4 supplied by Total (Courbevoie, France). ENGAGE is an ethylene-octene copolymer that performs well in a wide range of thermoplastic elastomer applications. The properties of the two polymers are reported in Table 1 and Table 2.

Table 1 Properties of ENGAGE 8445 as provided by the supplier.

Property	**Method**	**Unit**	**Typical value**
Melt Index (190 °C/2.16 kg)	ASTM D-1236	dg/min	3.5
Total Crystallinity	-	%	37

Melt Temperature	DSC Melting Peak (Rate 10 K/min)	°C	103
Glass Transition Temperature	DSC Inflection Point	°C	-38
Flexural Modulus (2 % Secant)	ASTM D-790	MPa	110.1
Density	ASTM D-792	g/cm^3	0.91

Table 2 Properties of EVA 1040 VN 4 as provided by the supplier.

Property	**Method**	**Unit**	**Typical value**
Melt Flow Rate (190 °C/2.16 kg)	ISO 1133	g/10 min	4.5
VA content	Total Petrochemicals	%	14
Melt Temperature	ISO 11357	°C	90
Vicat Temperature	ISO 306	°C	68
Elasticity Modulus	ISO 527-2	MPa	62
Density	ISO 1183	g/cm3	0.935

A masterbatch with 10 vol% (corresponding to 48.3 % by weight) of iron microparticles (particle size -325 meshes, assay 97 %), supplied by Sigma Aldrich (Saint Louis, Missouri, USA) was produced with each elastomer by means of a twin screw extruder. Subsequently, the masterbatch was diluted with neat polymer directly in the injection molding machine (a 70 ton CANBIMAT 65/185, from Negri-Bossi SpA, Italy) in order to obtain a compound with 2 % by volume of iron particles (corresponding to 14.6 % by weight). This final compound was used to produce both compact and foamed parts by means of the injection molding machine.

Rheological tests were performed by means of a Haake Mars rotational rheometer (Thermo Haake GmbH, Germany) on the blends to select the best processing conditions. These tests

were carried out at different temperatures (160 °C, 180 °C and 200 °C) thus obtaining the dependence of the complex viscosity, G' and G" on the oscillation frequency.

The exact weight percentage of iron powder present was checked on unfoamed samples and on both skin and core of foamed samples. A thermogravimetric analysis (TGA) by means of a Pyris Diamond TG/DTA from PerkinElmer (USA) was performed. Each sample was kept at 25 °C for 5 minutes and then heated at the rate of 5 K min^{-1} from 25 °C to 600 °C.

The injection molding machine adopted in this work presents a screw diameter of 25 mm and L/D = 22. The cylinder of the injection molding machine was modified to host a system for controlling the amount of gas injected during the batching phase. The screw was modified by introducing a mixing section in order to promote the fast solubilization of the blowing agent in the polymer melt. EVA and ENGAGE filled systems are referred to as EVA + Fe and ENGAGE + Fe, respectively.

The expressly designed mold consists of a hot runner, to avoid solidification inside the channels, with nozzle equipped with a needle valve to avoid premature foaming, and a system of electrical heaters specifically designed for the purpose of accurately controlling the temperature profile in the mold. The geometry of the cavity is shown in Figure 1.

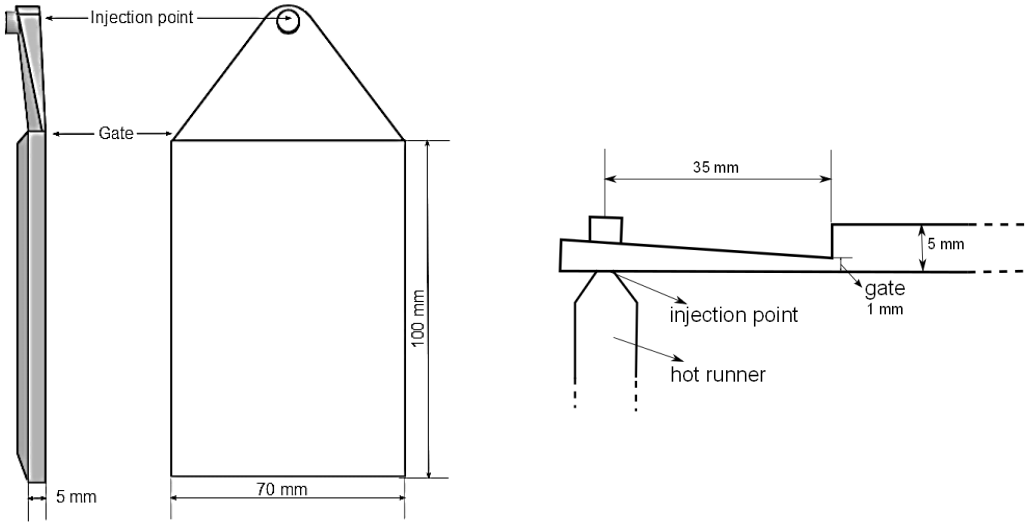

147

148 *(A)* *(B)*

149 Figure 1 (A) Geometry of the mold cavity used for the experiments; (B) particular of the

150 gate.

151

152 Experiments were performed on neat elastomers and their reinforced foams by solubilizing

153 nitrogen, which was injected at a pressure of 150 bar into the cylinder. The injection system

154 measures the mass of gas conveyed to the cylinder by monitoring the values of pressure and

155 volume before and after each gas injection. Experimental conditions, in particular temperature

156 profiles and injection flow rate, for each polymer are reported in Table 30 and were chosen in

157 order to obtain the best cellular morphology in neat polymer foams.

158

159 Table 3 Experimental conditions.

	ENGAGE	EVA
Temperature profile (°C)	190-200-220-220	180-190-200-200
Mold Temperature (°C)	35	35
Gas Pressure (bar)	150	250
Rotation Speed (rpm)	250	150
Shot Volume (cm3)	35	35
Injection Flow Rate (cm3/s)	7	14

160

161 Samples density at 25 °C was evaluated according to ASTM D792. The density reduction (*R*)
162 with respect to the unfoamed part was calculated according to equation (1), where ρ_0 is the
163 density of the unfoamed polymer and ρ_f is the density of the foamed part.

164 $$R = \frac{(\rho_0 - \rho_f)}{\rho_0} \quad (1)$$

165 In all cases, density measurements were performed on the whole molded sample previously
166 deprived of gate (the triangular part in Figure 1), in order to estimate the average density of
167 the sample. Subsequently, the same measurement was performed on four sections taken at
168 40 mm, 70 mm, 100 mm and 130 mm from the injection point in order to obtain a density
169 distribution along the flow path. The sections cut from the part were 70 mm x 10 mm x 5 mm
170 in size (as reported in the scheme of Figure 2-A).

171

172 *2.2 Methods*

173 Compressive and flexural tests were performed by means of a universal testing machine
174 (model CMT4304 from Shenzhen SANS Testing Machine Co. - China, now MTS - USA)
175 equipped with a 30 kN load cell. The compressive behavior was evaluated according to
176 ASTM D395 standard on specimens with dimensions of 50 mm x 20 mm x 5 mm (length x

177 width x thickness), cut at different distance from the injection point as indicated in Figure 2B.
178 A cross-head speed equal to 0.5 mm/min (strain rate equal to 0.1 min^{-1}) and a maximum strain
179 set at 0.30 mm/mm were used. Three-point bending tests were performed on neat and foamed
180 samples according to ASTM D790 standard, and a support span equal to 40 mm was used.
181 Five samples for each configuration were tested, and the average value and standard deviation
182 were evaluated.

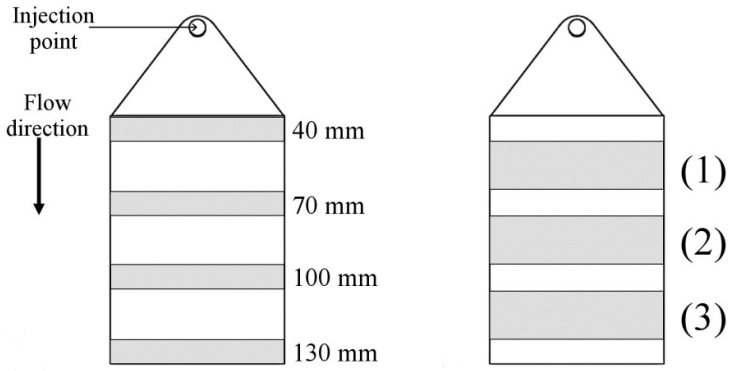

183
184 *(A)* *(B)*

185 Figure 2. Scheme of the parts cut at different distances from the injection point: (A)
186 samples for measuring density and (B) samples for mechanical and magneto-mechanical
187 characterization.

188

189 A specific tool was designed and set up to simultaneously apply a compressive load under a
190 magnetic field (MF) and evaluate the magneto-elastic properties of unfoamed and foamed
191 samples. The setup schematic is reported in Figure 3. It uses a universal testing machine
192 equipped with a 100 N load cell to measure the response of the sample during the MF
193 application. The frame used to compress the specimens was made of aluminum to avoid
194 interferences with the MF flux. The MF was applied by an electromagnetic C-shape dipole,
195 whose coil was powered by a high-speed bipolar amplifier BOP 50-20MG (KEPCO, Inc. –
196 USA) and controlled by means of a waveform generator TGA12104 (Aim-Tti, Thurlby

Thandar Instruments Limited – UK). The actual supplied current was measured by means a AC/DC current clamp (model i30s by Fluke Corporation – USA). The MF was measured by means of a transverse Hall probe (model HMMT-6J04-VR, Lake Shore Cryotronics, Inc. – USA) and a gaussmeter (model DSP 475, Lake Shore Cryotronics, Inc. – USA). All signals (force, current and magnetic field) were simultaneously recorded by means of an 18-bit analog-to-digital converter NI PCI-6289 (National Instruments Corporation, Austin, TX - USA) with a shielded I/O connector block NI SCB-68 (National Instruments Corporation, Austin, TX - USA).

The magneto-elastic characterization was evaluated by applying a pre-strain on the foams and then measuring the load under a uniform time-variable MF. To avoid stress relaxation phenomena, a 20 minutes time delay after the application of the pre-stain was awaited to stabilize the mechanical response of the foamed sample before the induction of the variable MF. The MF was then switched on at a frequency and amplitude equal to 0.05 Hz and 120 kA/m, respectively. The magneto-elastic characterization was carried out on samples 50 mm x 20 mm x 5 mm in size (length x width x thickness) cut at different distance from the injection point as indicated in Figure 2 B.

Also in this case five samples for each configuration were tested, and the average value and standard deviation were evaluated.

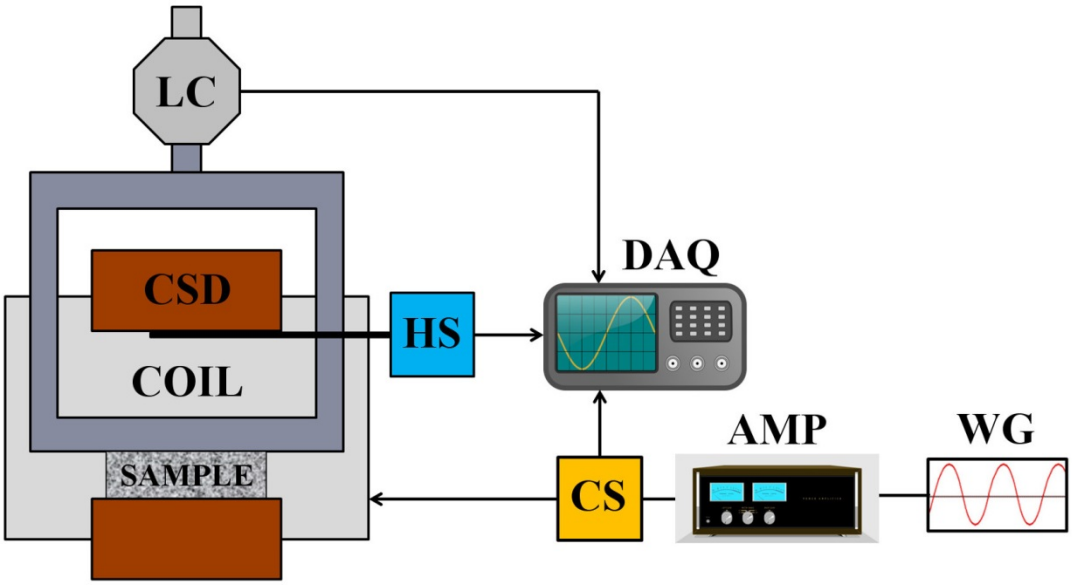

Figure 3. Sketch of the experimental setup for the magneto-mechanical characterization. LC: load cell; CSD: C-shape dipole; HS: Hall sensor; DAQ: data acquisition device; CS: electric current sensor; AMP: amplifier; WG: waveform generator.

3. RESULTS

3.1 Rheological characterization

Plots of the complex viscosity versus the oscillation frequency from rheological tests are shown in Figure 4 0A for ENGAGE and 4 0B for EVA. The comparisons between the complex viscosity at 180 °C of the neat and reinforced polymers (loaded with iron powder at 10 % by volume) are shown in Figure 5 A for ENGAGE and 5 B for EVA. The values of the thermal shift factor αT of all materials are reported in Table 4. From the graphs it is possible to observe that the presence of the filler induces a significant change in the rheological behavior. At high frequencies, the complex viscosity of the reinforced ENGAGE is lower than

that of the neat ENGAGE, while the complex viscosity of the reinforced EVA is always higher with respect to the neat EVA.

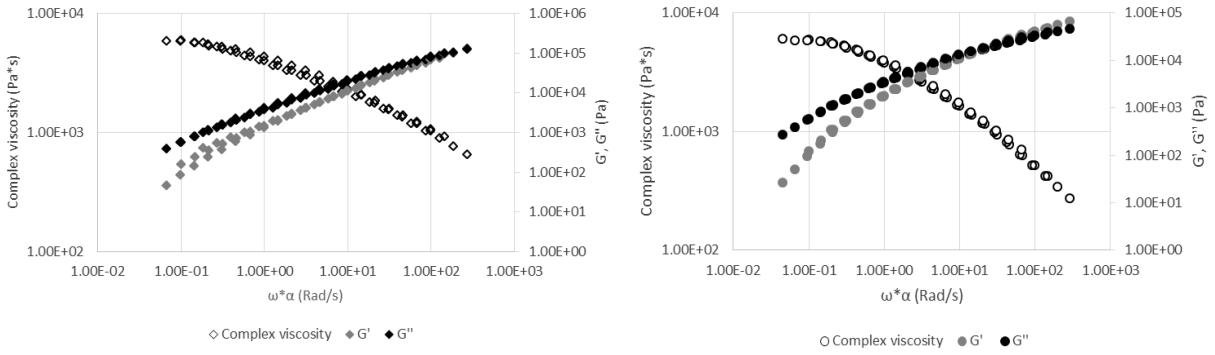

(A) *(B)*

Figure 4. Rheological properties neat ENGAGE (A) and EVA (B). Mastercurves at 180 °C.

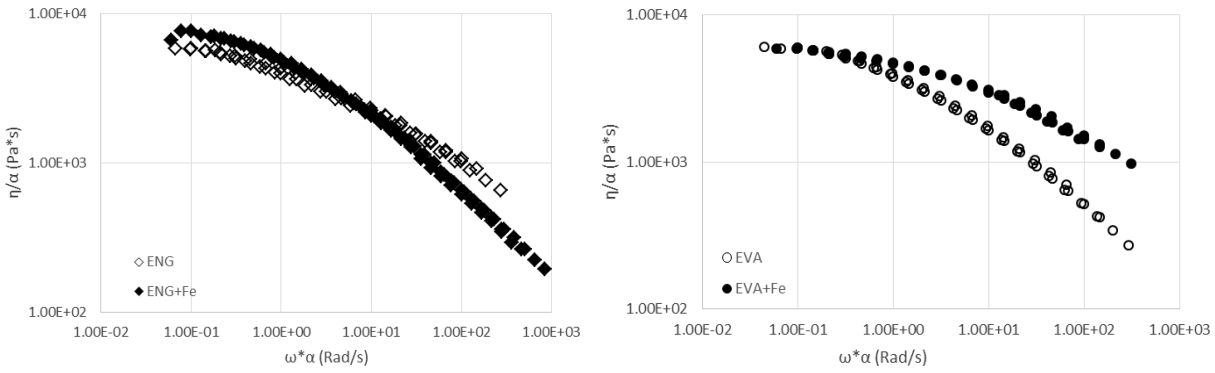

(A) *(B)*

Figure 5. Complex viscosity vs frequency of ENGAGE and EVA neat and with iron powder at 10 % by volume (Mastercurves at 180 °C)

Table 4 Thermal shift factors αT of ENGAGE and EVA

Temperature	**αT for ENG**	**αT for ENG+Fe**	**αT for EVA**	**αT for EVA+Fe**
160 °C	1.85	1.8	2	2.13
180 °C	1	1	1	1
200 °C	0.67	0.6	0.45	0.6

It is well known that for the neat materials adopted in this work the Cox-Merz rule is verified [17, 18], and thus the dependence of complex viscosity on the frequency, reported in Figures 4 and 5, is numerically the same of the dependence of the shear viscosity on the shear rate. Such condition allows to correctly describe the flow behavior of the material during the injection molding process. In order to check the validity of the Cox-Merz rule also for the polymers filled with iron powders, some further experiments were performed on the masterbatches (10 % by volume). In particular, rheological experiments at constant shear rate (0.1 and 1 s-1) were conducted in order to observe the steady shear viscosity during time [19]. In all cases it was observed that after few seconds the viscosity reaches a constant value that is similar (within differences of 15 %) to the corresponding value of complex viscosity obtained from the frequency sweep test at the corresponding oscillation frequency (0.1 and 1 rad/s, respectively). This suggests that in case of our filled materials the Cox-Mertz rule also applies at least up to shear rates in the transition from the Newtonian plateau to the power-law behavior. This is confirmed for the masterbatches, and can be thus assumed to be true for materials with a lower content of filler. Table 50 reports the values of steady shear viscosity and complex viscosity obtained on the ENGAGE and EVA masterbatches at the analyzed shear rates.

Table 5 Steady shear viscosity and complex viscosity of the ENGAGE and EVA masterbatches at 0.1 s^{-1} and 1 s^{-1}

Shear rate (s^{-1})/	**Steady shear viscosity (Pa*s)**		**Complex viscosity (Pa*s)**	
Frequency (rad/s)	*ENGAGE*	*EVA*	*ENGAGE*	*EVA*
0.1	8175	9500	7664	5992
1	5546	5326	4997	4733

3.2 Thermogravimetric analysis

Thermogravimetric analysis (TGA) was carried out on unfoamed samples and on skin and core of foamed samples in order to verify the exact weight percentage of iron present into the polymer. This analysis was also carried out on pellets of neat ENGAGE and EVA in order to establish their residual mass, to be subtracted from the residual mass from the TGA plots of reinforced samples.

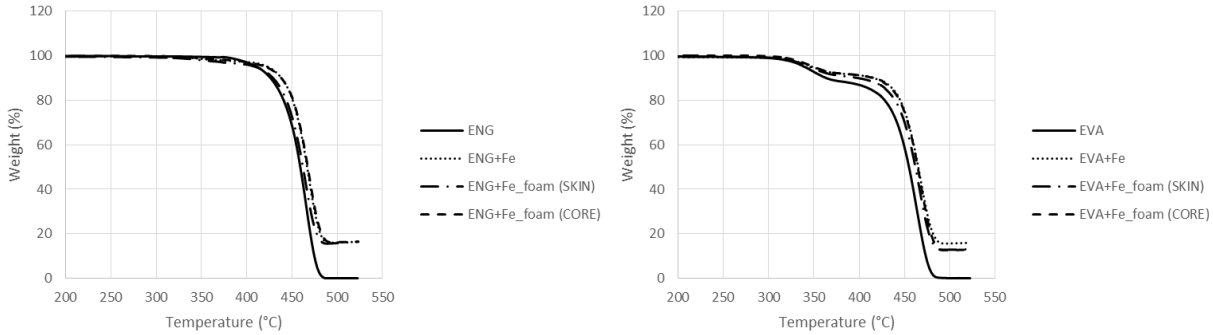

(A) *(B)*

Figure 6. Thermogravimetric analysis on samples of ENG+Fe (A) and EVA+ Fe (B).

The results of TGA (Figure 60) show a residue equal to zero for neat ENGAGE and neat EVA. All samples of ENGAGE reinforced with iron particles show a residue of about 16.4 % by weight, corresponding to 2.2 % by volume. The residual mass of the reinforced EVA was 13.3 % by weight, corresponding to 1.8 % by volume, while the foamed EVA + Fe showed a slightly lower residue. The composite blends have shown an amount of Fe particles within ± 10 % of the target value.

3.3 Morphology

The density reduction of reinforced polymers and their foams are reported in Table 6 for ENGAGE and EVA based systems, respectively. The data are average values of three measurements per condition.

Table 6. Density reduction of ENG_foam, ENG+Fe_foam, EVA_foam and EVA+Fe_foam at different distances from the injection point.

Distance from the injection point (mm)	**ENG_foam**	**ENG+Fe_foam**	**EVA_foam**	**EVA+Fe_foam**
40	35.053 ± 1.052	32.734 ± 1.146	35.328± 0.883	26.251± 1.155
70	35.054 ± 1.087	34.992 ± 1.155	34.968 ± 0.944	33.331 ± 1.499
100	30.536 ± 1.099	34.561 ± 1.244	29.965 ± 0.899	32.288 ± 1.195
130	34.422 ± 0.998	37.414 ± 1.160	34.552 ± 0.760	36.023 ± 1.441

For both systems, the density reduction of foamed reinforced samples slightly increased with the distance from the injection point. This trend is more evident in EVA based samples, while ENGAGE based systems showed a more homogeneous density. Furthermore, ENGAGE + Fe foams showed a slightly higher density reduction (hence a lower density) with respect to EVA + Fe ones.

Optical micrographs from the different sections of unfilled and filled ENGAGE foams are shown in Figure 70. The addition of a small amount of iron particles allowed a marked improvement in the cellular morphology. The different morphology was the reason why foams from neat ENGAGE showed a slightly higher density at 40 mm from the injection point with respect to reinforced ENGAGE foams. In fact, at 40 mm from the injection point the neat ENGAGE sample shows the typical core-skin morphology, with the core exhibiting

few but large cells. The cellular morphology of reinforced ENGAGE foam is very fine and regular throughout the sample length, with many small cells.

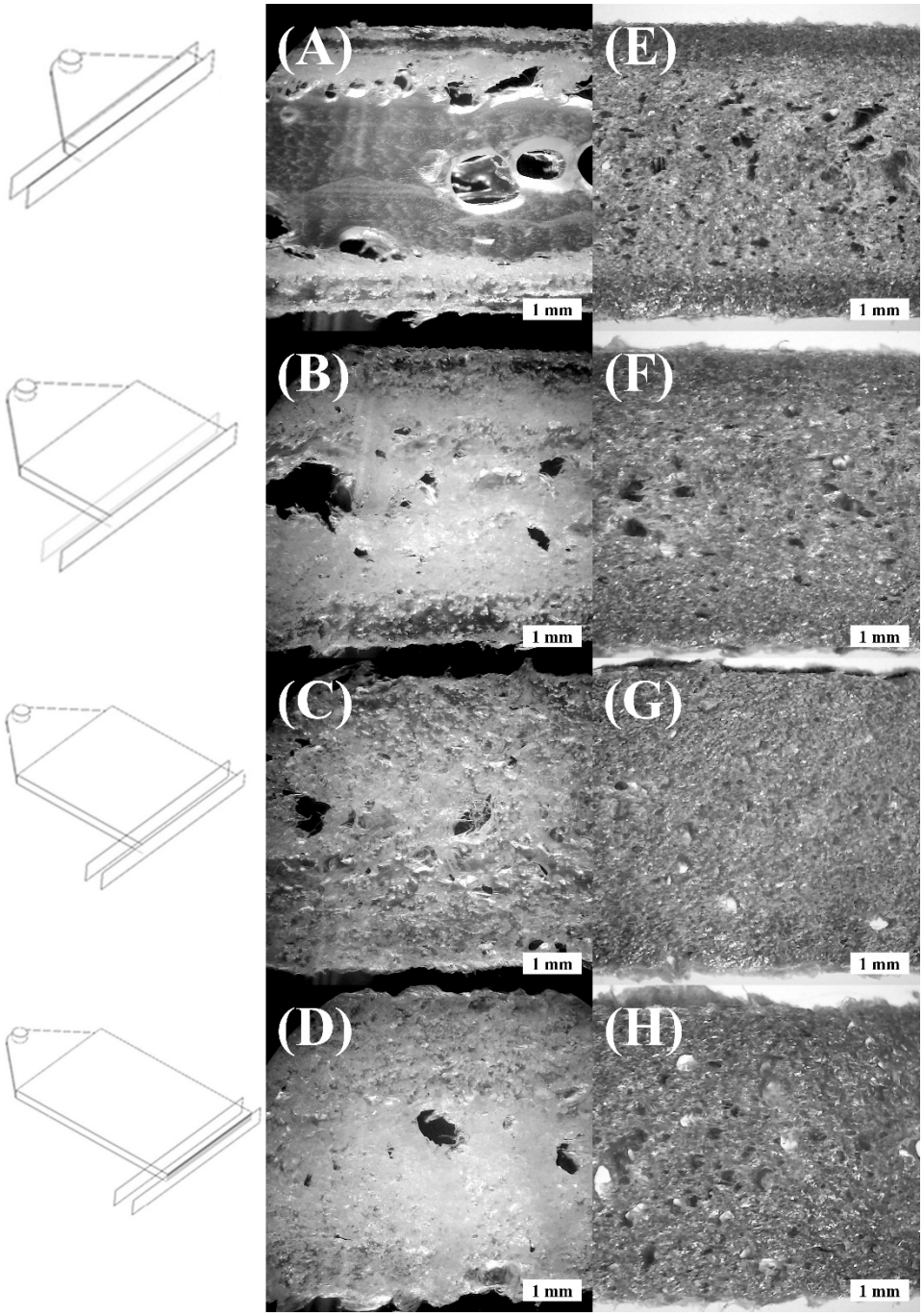

Figure 7. Optical micrographs at different distances from the injection point: (A-D) ENG_foam samples and (E-H) ENG+Fe_foam.

303

304 The same comparison was made between EVA based foams (Figure 80). Also in this case, a
305 great improvement of the cellular morphology was detected in reinforced foams. In fact, in
306 the core layer of reinforced EVA there are no more compact zones as in neat EVA, even if
307 some large voids are still present in the core region, differently from the case of reinforced
308 ENGAGE.

309

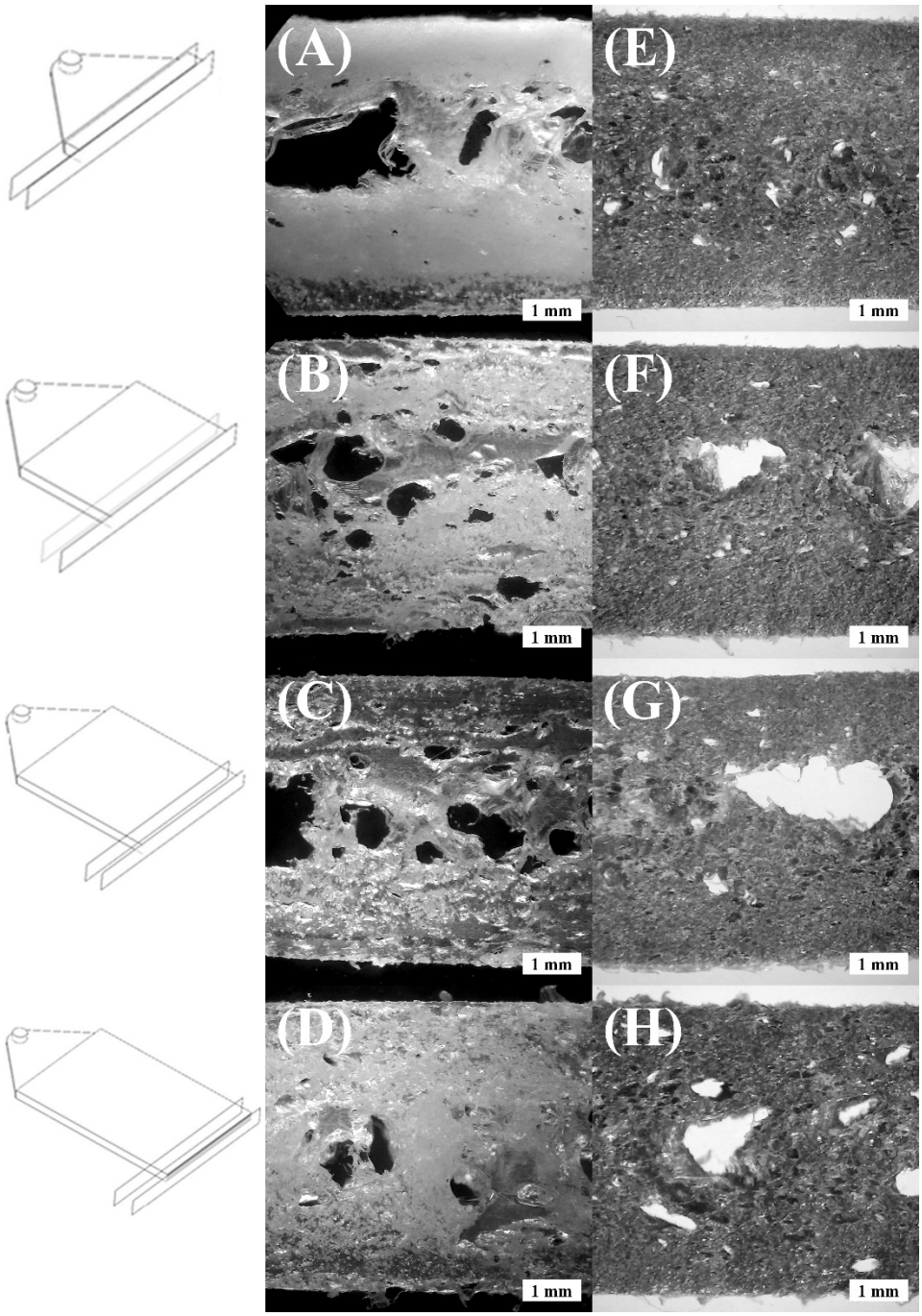

Figure 8. Optical micrographs acquired by the optical microscope at different distances from the injection point: (A-D) EVA_foam samples and (E-H) EVA+Fe_foam ones.

3.4 Mechanical behavior analysis

The morphology developed during the injection foaming has a significant role in the mechanical behaviour. Representative stress-strain curves from compressive and flexural tests for ENGAGE and EVA systems are shown in Figure 9 and Figure 10, respectively, while average values and standard deviations of compressive and flexural moduli are summarized in Table 7. The presence of particles did not significantly influence the mechanical behaviour of ENGAGE and EVA based systems, and ENGAGE ones showed a higher standard deviation in bending tests. The presence of particles in ENGAGE based foams promotes the formation of an even cellular structure, and reduces the thickness of the skins. This translates in a higher compressive performance (mainly affected by the core) and a lower bending stiffness (due to the lower skin thickness). In EVA based foams, the cellular structure is similar with and without the particles and this renders the performance of reinforced and not reinforced foams almost equal. It is worth to note that samples performances are affected by a significant variance, as typical for injection molded foams.

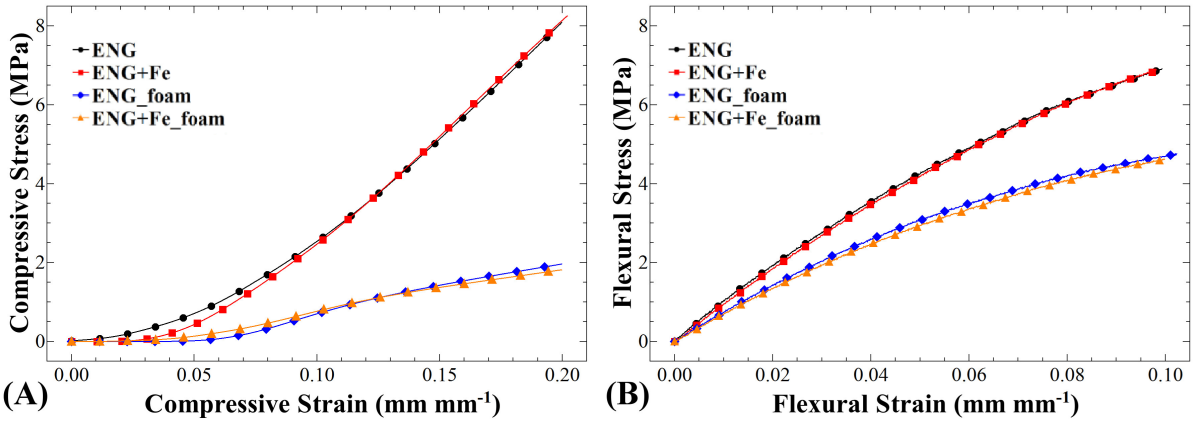

Figure 9. Stress-strain curves for samples with ENGAGE: (A) compression and (B) bending.

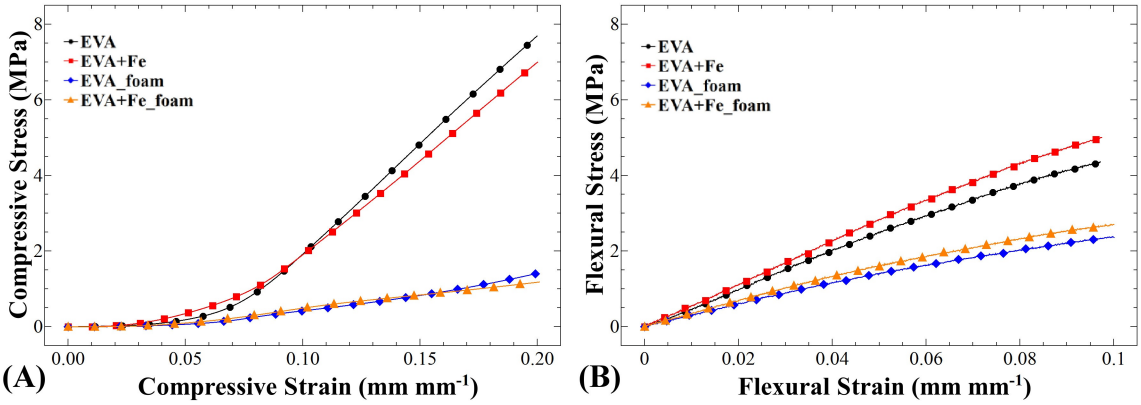

Figure 10. Stress-strain curves for samples with EVA: (A) compression and (B) bending.

Table 7. Density, compressive and flexural moduli of tested systems.

Sample	**Density (g cm^{-3})**	***E*$_{comp}$ (MPa)**	***E*$_{flex}$ (MPa)**
ENG	0.838 ± 0.007	48.44 ± 3.23	76.51 ± 3.61
ENG+Fe	0.988 ± 0.003	53.14 ± 4.73	79.61 ± 2.97
ENG_foam	0.609 ± 0.070	17.89 ± 5.55	53.69 ± 9.19
ENG+Fe_foam	0.644 ± 0.047	18.32 ± 2.14	49.54 ± 11.91
EVA	0.891 ± 0.011	55.87 ± 1.85	51.51 ± 1.74
EVA+Fe	1.004 ± 0.020	53.47 ± 3.00	62.72 ± 3.05
EVA_foam	0.667 ± 0.028	12.84 ± 3.86	30.80 ± 3.19
EVA+Fe_foam	0.647 ± 0.024	12.25 ± 2.19	31.52 ± 2.88

3.5 Magneto-elastic behavior

The main feature of the composite materials presented in this paper is the magneto-elastic behaviour under the magnetic field (butterfly effect). In the magneto-elastic characterization, a fixed pre-strain was applied to samples before the application of a uniform time-variable

MF. Both the MF and the strain were applied along the thickness direction. Different pre-strains were applied to the sample to investigate the effect of pre-strain on the magneto-elastic behaviour. The force variation induced by the application of the MF, which superimposed to the static response, was recorded.

As expected, neat systems (both unfoamed and foamed) did not show any force variation under the MF, as a result of the lack of interactions of the polymer with it. On the contrary, reinforced samples exhibited a consistent sensitivity to MF. In Figure 11 the magneto-elastic response of the EVA+Fe_foam sample under a sine waveform MF at different pre-strain is shown. The static stress (dotted straight lines) was due to the application of the pre-strain. It is shown as reference value to evidence the force change during the MF application. The presence of MF induced a change of the detected compressive stress (solid coloured lines), precisely following the MF signal changes (solid grey lines). The stress variation during the MF application was always negative and its plot is below the reference static stress. Minima of the stress curve were reached in occurrence of each minimum and maximum of the MF signal. Since the strain was kept constant during the magneto-elastic characterization, the resulting stress was a combination of the MF-induced stress with the mechanical compressive response.

The stress variation under MF was in inverse proportion with the pre-strain and became positive at 0.04 mm/mm. It is worth mentioning that the stress variation was independent of the MF direction and it depended only on its amplitude, as reported in Figure 12. Indeed, when the direction of the MF was reversed (negative MF values), the stress showed a reduction trend similar to that showed in case of positive MF values. This phenomenon is represented by the butterfly-shaped curves, which are congruent with the magneto-elastic behaviour of high density, iron filled solid materials. The positive values can be explained

with the fact that at this pre-strain the aligned structures are buckled and under the magnetic field they tend to recover the linear shape.

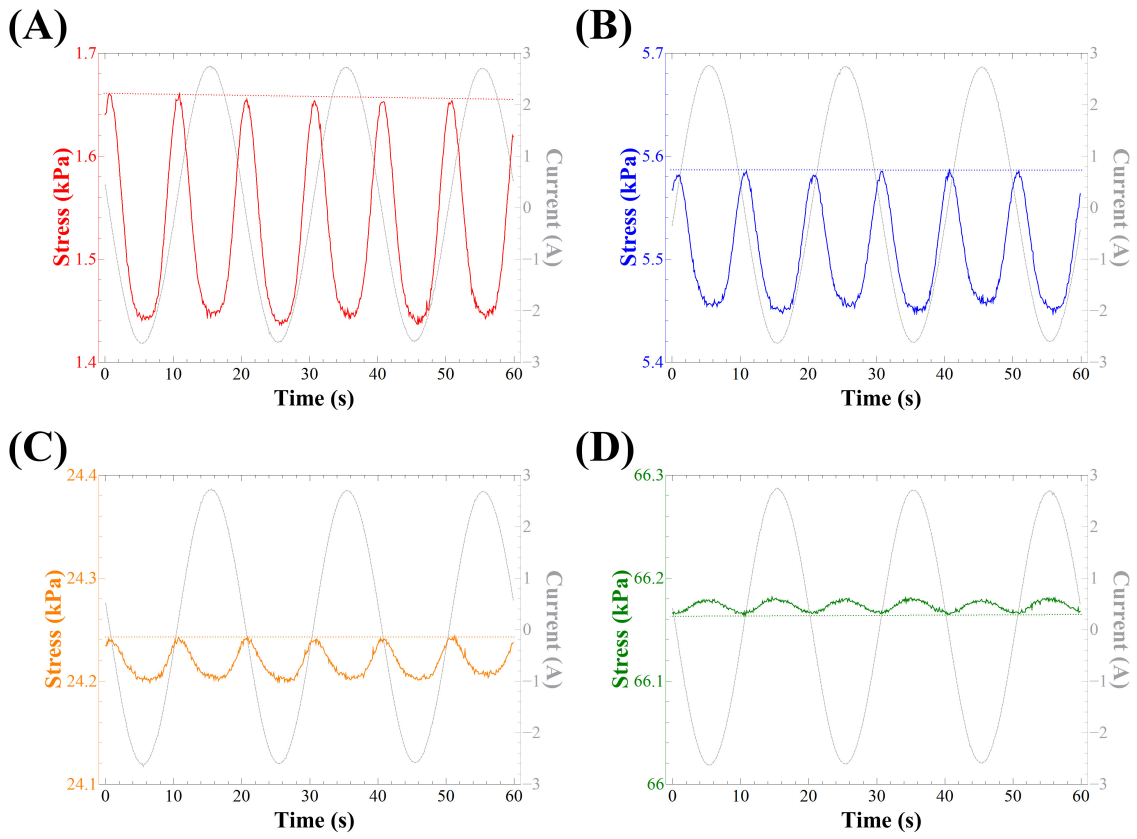

Figure 11. Magneto-mechanical tests of the sample EVA+Fe_foam(3) at different pre-strain: (A) 0.01 mm/mm; (B) 0.02 mm/mm; (C) 0.03 mm/mm; (D) 0.04 mm/mm.

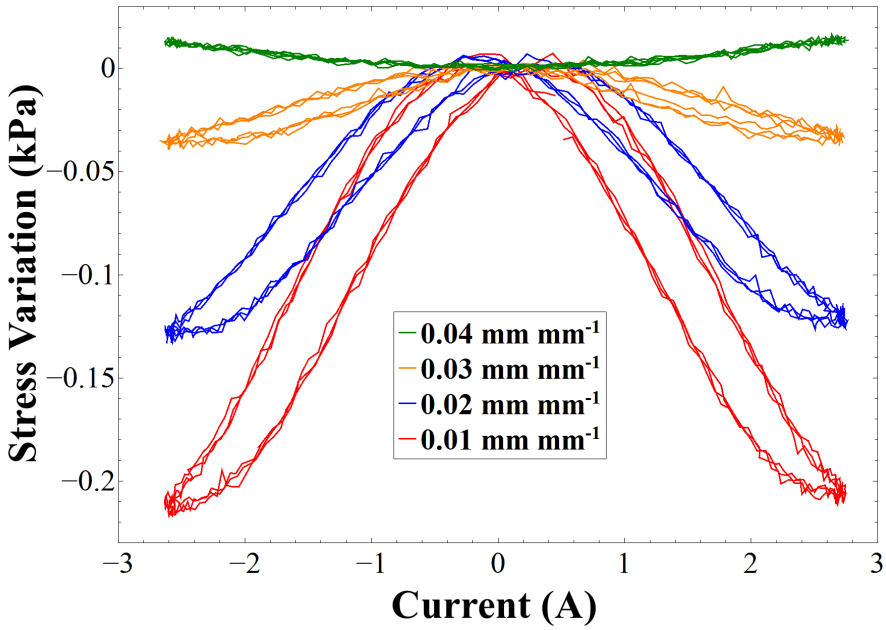

Figure 12. Magnetic-field-induced stress variation of EVA+Fe_foam (3) sample at different pre-strains.

Such results can be considered as an apparent change of the material stiffness, similarly to the so called *ΔE-effect* (variation of the elastic modulus) reported on magneto-strictive materials. According to the microscopic approach in modelling the magneto-elastic behaviour, this stress variation is due to the pair-wise interactions between magnetic moments of particles developed in iron particles under the application of a magnetic field [20]. The particle-particle interactions can lead to their attraction (typically between particles positioned along the MF lines) or repulsion (typically between particles in orthogonal direction to the MF), with an intensity depending on their mutual position and distance. In Figure 13 a graphical representation of particle interactions is reported. The proportional reduction of the measured stress with the MF strength, for pre-strains from 0.01 mm/mm to 0.03 mm/mm, with respect to the reference value is an indirect evidence that the prevailing effect is attractive, hence particles interactions help in compressing the foam. Samples pre-strained at 0.03 mm/mm and

0.04 mm/mm, for unfoamed and foamed samples respectively, did not show a stress reduction but a stress increase with respect to the reference stress under MF. This behaviour has been detected in previous works in samples with a particle distributed along preferential directions (in foams with long linear aggregates of particles), hence further investigation is needed to understand why such behaviour has been detected in systems with randomly dispersed particles [21-23].

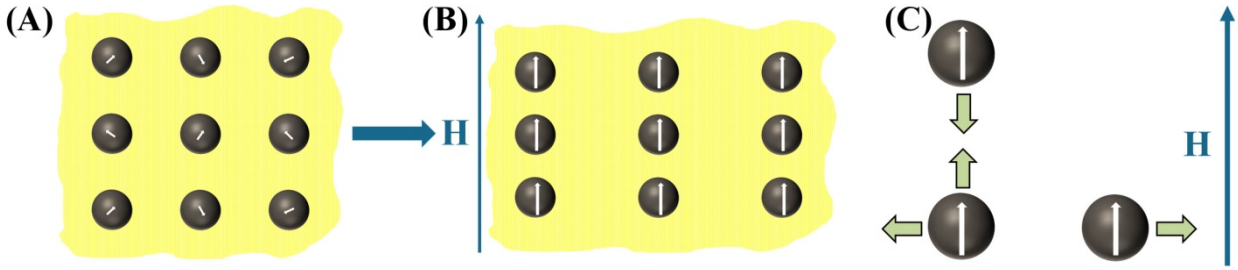

Figure 13. Sketch of particle-particle interactions in a magneto-sensitive material with magnetic particles arranged on the sites of a regular rectangular lattice: (A) without MF and (B) applying an external MF. (C) Interaction of magnetic particles depending on their mutual positions (redrawn from [29]).

In Figure 14 A comparison between the magneto-elastic performance of unfoamed and foamed samples for EVA and ENGAGE systems under a pre-strain equal to 0.01 mm/mm is reported. The EVA+Fe_foam sample showed a stress variation higher than EVA+Fe one. The ENG+Fe and ENG+Fe_foam samples, on the contrary, exhibited a similar behaviour. In Table 8 the results of the magneto-elastic characterization performed on both solid and foamed systems are reported in terms of stress variation as a function of the pre-strain value. EVA+Fe_foam samples showed a magneto-elastic response higher than the unfoamed analogous, demonstrating that foams reinforced with magnetic particles produced by an injection molding process behave in the same way like systems based on polyurethane foams

409 reinforced with magnetic micro-particles [22]. Furthermore, low density magneto-sensitive
410 materials can be produced with thermoplastics by using the injection molding process.

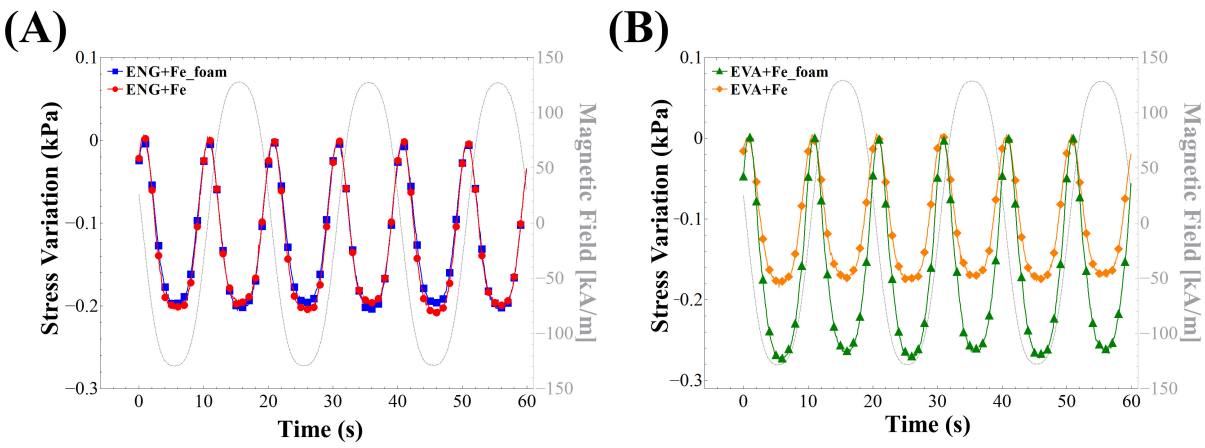

411

412 Figure 14. Magneto-mechanical comparison between unfoamed and foamed samples at the
413 pre-strain equal to 0.01 mm mm-1: (A) ENGAGE and (B) EVA.

414

Table 8. Mean value and standard deviation of stress variation (data are reported in kPa) in magneto-mechanical tests at different pre-strains (expressed in mm mm^{-1}).

Sample	**ε = 0.01**	**ε = 0.02**	**ε = 0.03**	**ε = 0.04**
ENG+Fe(1)	-0.203 ± 0.004	-0.057 ± 0.003	**+0.072 ± 0.001**	**- - -**
ENG+Fe(2)	-0.149 ± 0.003	-0.041 ± 0.004	**+0.132 ± 0.003**	**- - -**
ENG+Fe(3)	-0.217 ± 0.007	-0.057 ± 0.003	**+0.094 ± 0.002**	**- - -**
ENG+Fe_foam(1)	-0.192 ± 0.004	-0.045 ± 0.001	-0.018 ± 0.002	**+0.032 ± 0.001**
ENG+Fe_foam(2)	-0.149 ± 0.006	-0.105 ± 0.003	-0.018 ± 0.003	**+0.032 ±0.003**
ENG+Fe_foam(3)	-0.199 ± 0.004	-0.119 ± 0.003	-0.013 ± 0.002	**+0.033 ±0.002**
EVA+Fe(1)	-0.182 ± 0.003	-0.021 ± 0.001	**+0.018 ± 0.001**	**- - -**
EVA+Fe(2)	-0.177 ± 0.003	-0.019 ± 0.002	**+0.008 ± 0.002**	**- - -**
EVA+Fe(3)	-0.156 ± 0.003	-0.037 ± 0.001	**+0.020 ± 0.001**	**- - -**
EVA+Fe_foam(1)	-0.312 ± 0.006	-0.221 ± 0.006	-0.033 ± 0.003	**+0.014 ± 0.003**
EVA+Fe_foam(2)	-0.268 ± 0.004	-0.170 ± 0.003	-0.067 ± 0.002	**+0.007 ± 0.001**

4. CONCLUSIONS

The effect of iron microparticles on thermoplastic elastomers was analyzed in order to evaluate the feasibility of producing low density magneto-sensitive materials by using the injection molding technique. The effect of the iron microparticles on the foaming process and cellular morphology was also investigated. In particular, reinforced foams were prepared by using thermoplastic elastomers (EVA and ENGAGE) loaded with 2 % by volume of iron powder. Compact and foamed parts were produced by means of an injection molding machine, and the magneto-elastic behavior of samples under the application of a magnetic field was investigated.

The use of iron micro-particles allowed a remarkable improvement of the cellular morphology of samples, molded at the same conditions. In fact, the addition of a small percentage of iron

429 powder induced a strong increase of the number of nucleated cells without increasing the final
430 density. At small distances from the injection point, samples of neat ENGAGE showed a
431 compact skin, a foamed zone between the skin and the core layer, and a core with a lot of
432 unfoamed zones and large cells, which contributed to increase the density. Samples of
433 ENGAGE with iron powder have a good and homogeneous foaming both in the transition
434 zone and in the core already at small distances from the injection point. The mechanical
435 (compressive and flexural) performances were not significantly influenced by the particle
436 presence, both in solid and foamed systems.
437 The magneto-mechanical characterization, performed by applying a fixed strain and a uniform
438 magnetic field with a sine waveform and then measuring the response in terms of stress
439 variations, showed an apparent reduction of the elastic modulus of the foams due to the
440 interactions between the particles and the applied magnetic field. In fact, samples having a
441 random particle distribution showed a negative, proportional to the applied magnetic field
442 variation of the compressive stress. Such behavior demonstrated that magneto-sensitive
443 porous materials made of thermoplastics can be produced by means of the injection molding
444 process.

445 **5. ACKNOWLEDGMENTS**

446 These research activities were supported by the Italian Ministry of Education and Research
447 (MIUR) within the PRIN project *Developing polymeric smart foams with behaviour*
448 *controlled by the magnetic field* – E.PO.CA.M. (grant number PRIN 2012JWPMN9). Authors
449 would like to thank Mr Fabio Docimo for its contribution to the preparation of all tested
450 samples.

REFERENCES

[1] L. Sorrentino, M. Aurilia, G. Forte, S. Iannace, Composite polymeric foams produced by using magnetic field, in: Advances in Science and Technology, Trans Tech Publ, 2008, pp. 123-126.

[2] D. Borin, D. Günther, C. Hintze, G. Heinrich, S. Odenbach, The level of cross-linking and the structure of anisotropic magnetorheological elastomers, Journal of Magnetism and Magnetic Materials, 324 (2012) 3452-3454.

[3] M. Krautz, D. Werner, M. Schrödner, A. Funk, A. Jantz, J. Popp, J. Eckert, A. Waske, Hysteretic behavior of soft magnetic elastomer composites, Journal of Magnetism and Magnetic Materials, 426 (2017) 60-63.

[4] C. Tovar-Cisneros, R. Gonzalez-Nunez, D. Rodrigue, Effect of mold temperature on morphology and mechanical properties of injection molded HDPE structural foams, J Cell Plast, 44 (2008) 223-237.

[5] A.N.J. Sporrer, V. Altstadt, Controlling morphology of injection molded structural foams by mold design and processing parameters, J Cell Plast, 43 (2007) 313-330.

[6] R. Pantani, A. Sorrentino, V. Volpe, G. Titomanlio, Foam Injection Molding of Poly(Lactic Acid) with Physical Blowing Agents, Aip Conf Proc, 1593 (2014) 397-400.

[7] Z.H. Xi, J. Chen, T. Liu, L. Zhao, L.S. Turng, Experiment and simulation of foaming injection molding of polypropylene/nano-calcium carbonate composites by supercritical carbon dioxide, Chinese J Chem Eng, 24 (2016) 180-189.

[8] P. Svoboda, C.C. Zeng, H. Wang, L.J. Lee, D.L. Tomasko, Morphology and mechanical properties of polypropylene/organoclay nanocomposites, J Appl Polym Sci, 85 (2002) 1562-1570.

[9] H.M. Tiggemann, V.F. Ribeiro, F. Celso, S.M.B. Nachtigall, Effect of commercial clays on the properties of SEBS/PP/oil thermoplastic elastomers. Part 1. Physical, mechanical and thermal properties, Appl Clay Sci, 109 (2015) 151-156.

[10] X.L. Gong, C.Y. Guo, S.H. Xuan, T.X. Liu, L.H. Zong, C. Peng, Oscillatory normal forces of magnetorheological fluids, Soft Matter, 8 (2012) 5256-5261.

[11] J.D. Carlson, M.R. Jolly, MR fluid, foam and elastomer devices, Mechatronics, 10 (2000) 555-569.

[12] M.R. Jolly, J.D. Carlson, B.C. Munoz, A model of the behaviour of magnetorheological materials, Smart Mater Struct, 5 (1996) 607-614.

[13] Y.L. Raikher, O.V. Stolbov, Numerical modeling of large field-induced strains in ferroelastic bodies: a continuum approach, J Phys-Condens Mat, 20 (2008).

[14] A.P. Safronov, T.V. Terziyan, A.S. Istomina, I.V. Beketov, Swelling and Contraction of Ferrogels Based on Polyacrylamide in a Magnetic Field, Polym Sci Ser a+, 54 (2012) 26-33.

[15] V. Volpe, M. D'Auria, L. Sorrentino, D. Davino, R. Pantani, Injection molding of magneto-sensitive polymer composites, Materials Today Communications, 15 (2018) 280-287.

[16] M. Schrödner, G. Pflug, Magnetomechanical properties of composites and fibers made from thermoplastic elastomers (TPE) and carbonyl iron powder (CIP), Journal of Magnetism and Magnetic Materials, 454 (2018) 258-263.

[17] S. Paul, D.D. Kale, Rheological study of polypropylene copolymer/polyolefinic elastomer blends, J Appl Polym Sci, 84 (2002) 665-671.

[18] S. Hui, T.K. Chaki, S. Chattopadhyay, Dynamic and Capillary Rheology of LDPE-EVA-Based Thermoplastic Elastomer: Effect of Silica Nanofiller, Polym Composite, 31 (2010) 377-391.

[19] R.R. Tiwari, D.R. Paul, Polypropylene-elastomer (TPO) nanocomposites: 1. Morphology, Polymer, 52 (2011) 4955-4969.
[20] L. EW, Magnetostriction and Magnetomechanical Effects, Reports on Progress in Physics, 18 (1955).
[21] A.E. Clark, M. Wun-Fogle, J.B. Restorff, T.A. Lograsso, Magnetostrictive properties of galfenol alloys under compressive stress, Mater Trans, 43 (2002) 881-886.
[22] M. D'Auria, D. Davino, R. Pantani, L. Sorrentino, Polymeric foam-ferromagnet composites as smart lightweight materials, Smart Materials and Structures, 25 (2016).
[23] D. Ivaneyko, V. Toshchevikov, D. Borin, M. Saphiannikova, G. Heinrich, Mechanical Properties of Magneto-Sensitive Elastomers in a Homogeneous Magnetic Field: Theory and Experiment, Macromol Symp, 338 (2014) 96-107.